International Journal of Microwave and Wireless Technologies

cambridge.org/mrf

A compact 12 × 12 MIMO loop antenna for 5G mobile phone applications

Ji-Peng Jhuang[1] and Hsin-Lung Su[2]

[1]Department of Computer Science and Information Engineering, National Pingtung University, Pingtung, Taiwan and [2]Department of Computer and Communication, National Pingtung University, Pingtung, Taiwan

Research Paper

Cite this article: Jhuang JP, Su HL (2024) A compact 12 × 12 MIMO loop antenna for 5G mobile phone applications. *International Journal of Microwave and Wireless Technologies* **16**(1), 151–161. https://doi.org/10.1017/S1759078723000673

Received: 27 January 2023
Revised: 07 May 2023
Accepted: 09 May 2023

Keywords:
5G antennas; compact antennas; loop antennas; MIMO antenna array; mobile phone antennas

Corresponding author: Hsin-Lung Su; Email: hlsu@mail.nptu.edu.tw

Abstract

A compact 12-element multiple-input multiple-output loop antenna array for a fifth-generation (5G) mobile phone is proposed. The operating band for the proposed antenna covers the long-term evolution 42 band, which spans a frequency range of 3.4–3.6 GHz. The size of the single antenna element is 5.85 × 4.9 mm^2 ($0.068\lambda_0 \times 0.057\lambda_0$), and 12 of these elements are positioned along two side edges of the mobile phone. This antenna is suitable for high screen-to-body ratio devices. The measured 6-dB impedance bandwidth is from 3.4 to 3.73 GHz. The measured total efficiency of the proposed antenna is 39–56% and the peak gain is 0–3.2 dBi. The transmission coefficient is less than −12 dB, the envelope correlation coefficient is less than 0.42, and the channel capacity is 45–50 bps/Hz.

Introduction

Fifth-generation (5G) mobile communication has three features: Ultra-Reliable and Low Latency Communications, Enhanced Mobile Broadband, and Massive Machine Type Communications. In release technical specification, 38 of the 3 GPP, 5G mobile communications operating bands are in the Sub-6-GHz band (410–7125 MHz) [1–28]. The European Commission has designated a frequency range of 3.4–3.8 GHz specifically for the deployment of 5G technology [5]. The 3.5-GHz (3.4–3.6 GHz) frequency band is now the most commonly used frequency band [3–18]. Multi-input multi-output (MIMO) technology is used to increase data transmission speed. MIMO technology uses spatial diversity to increase data transmission speed [19]. MIMO technology does not require extra bandwidth or transmission power and significantly increases channel capacity (CC) and spectral efficiency. Therefore, MIMO technology is critical for 5 G communication systems [1–28].

Antenna types include inverted-F, open slot, patch, fractal geometry, and loop [6, 18, 20–22]. There are many types of MIMO antennas because fractal geometry and loop antennas have a small footprint, are inexpensive, have a simple structure, and allow easy impedance matching [8–11]. A previous study [18] arranged eight antennas on the two long side edges and printed them on the inner and outer surfaces of the frame. An I-shaped feeding part and a modified Hilbert fractal monopole antenna comprise the structure of the antenna. The Hilbert space-filling property is used to achieve significant miniaturization. Loop antennas also have a variety of shapes, such as circles, triangles, and rectangles, all of which have similar far-field patterns. A loop antenna can be coupled through the feeding structure on the inner surface to reduce the size of the antenna so a fractal geometry and a loop antenna can be used for a mobile phone with a high screen-to-body ratio [9, 10, 13, 18].

Antennas in the MIMO antenna system must be isolated, but mobile phones are becoming more compact so mutual coupling is increased. Mutual coupling results in poor isolation and a low data transmission rate. Physical separation, a metasurface [1, 2], a one-wavelength mode [6], self-decoupling [10], a single common grounding branch [15], decoupling structures [17], a neutralized line [23], diverse polarization [3, 5, 7, 24], and a decoupling network [25] are used to increase isolation. A metasurface, a common grounding branch, decoupling structures, a neutralized line, and a decoupling network require additional elements. Self-decoupling, a single common grounding branch, and diverse polarization require more ground plane space.

This study proposes a 12 × 12 MIMO antenna array that requires no external passive elements. The proposed single-loop antenna element has a compact uniplanar structure with a footprint of 5.85 × 4.9 mm^2 ($0.068\lambda_0 \times 0.057\lambda_0$). Table 1 shows a comparison between the proposed antenna and those of other studies. The proposed antenna has the smallest dimensions, so it is suitable for a mobile phone with a high screen-to-body ratio. The transmission coefficient for the proposed antenna is less than −12 dB without any decoupling structure between

© The Author(s), 2023. Published by Cambridge University Press in association with the European Microwave Association

Table 1. Comparison between the proposed antenna and those of other studies

References	6-dB bandwidth (GHz)	Size ($L \times W \times H$)	MIMO order	Transmission coefficient (dB)	GRND clearance (mm)	Efficiency (%)
[9]	3.4–3.6	6.5 × 6 × 0.8 mm^3	10	<−10	1	>65
[10]	3.4–3.6	21 × 3 × 5 mm^3	8	<−20	0	>56
[12]	2.38–2.72 and 3.19–3.84	16 × 15 mm^2	6	<−15	16	86–92
[8]	3.4–3.6	3.1 × 10 mm^2	8	<−10	1	>40
[13]	3.4–3.6 and 4.8–5.1	7 × 15 mm^2	8	<−11.5	0	40–85
[14]	3.38–3.66 and 4.3–5.18	16.5 × 5.5 mm^2	10	<−12.5	3	42–80
[18]	3.4–3.6	9.57 × 5.99 mm^2	8	<−12.2	0	65–75
[*]	3.4–3.6	5.85 × 4.9 mm^2	12	<−12	0	39–56

* The proposed antenna

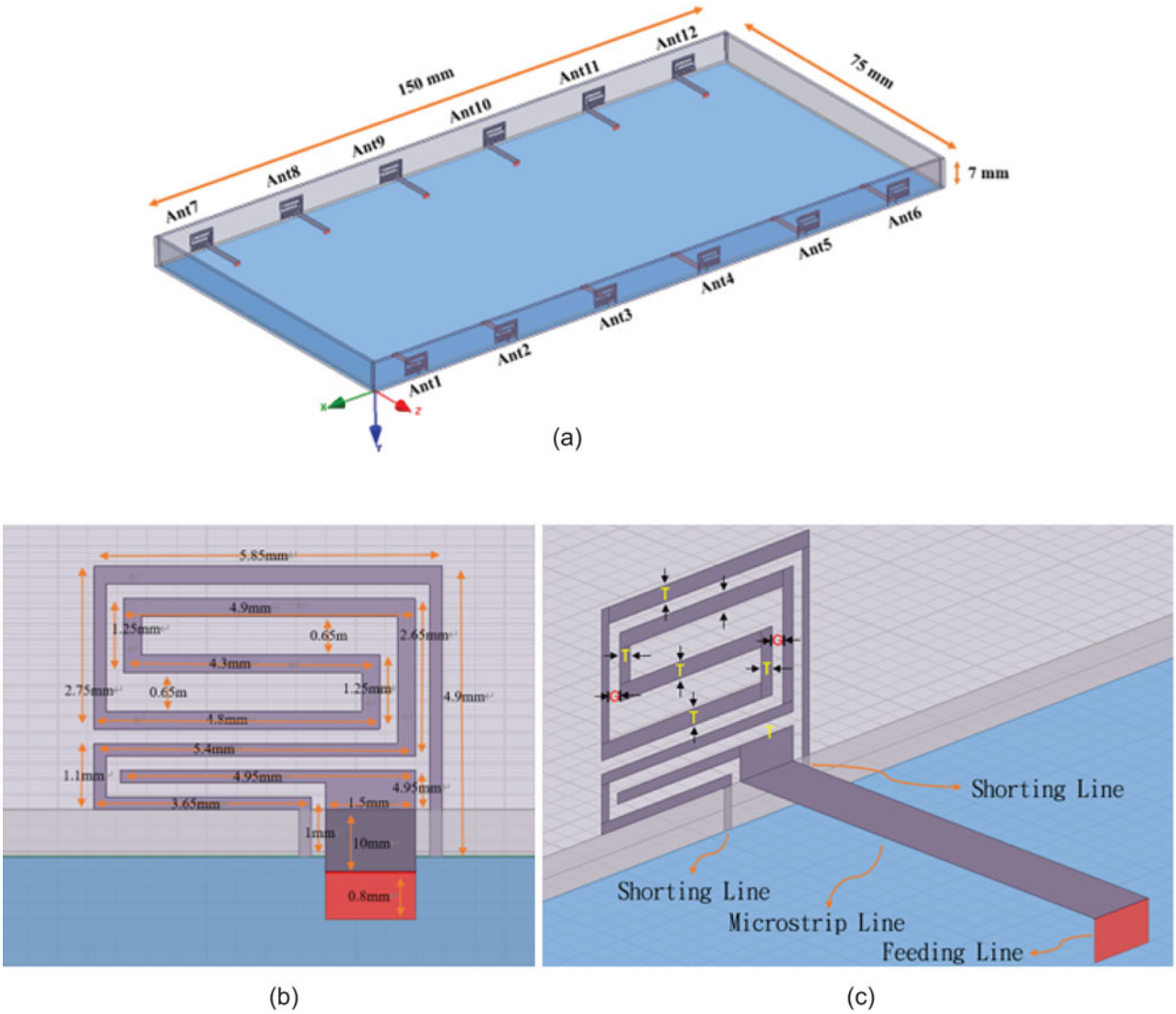


Figure 1. (a) The position of the MIMO antenna array in a mobile phone; the detail parameters for the proposed single antenna element in (b) the front view and (c) the lateral view.

https://doi.org/10.1017/S1759078723000673 Published online by Cambridge University Press

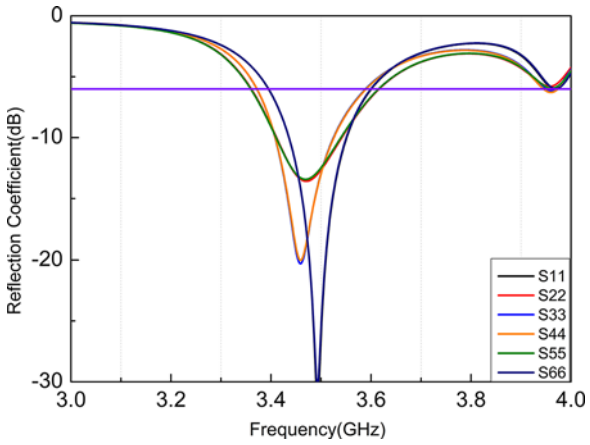


Figure 2. Reflection coefficients for the proposed MIMO antenna array.

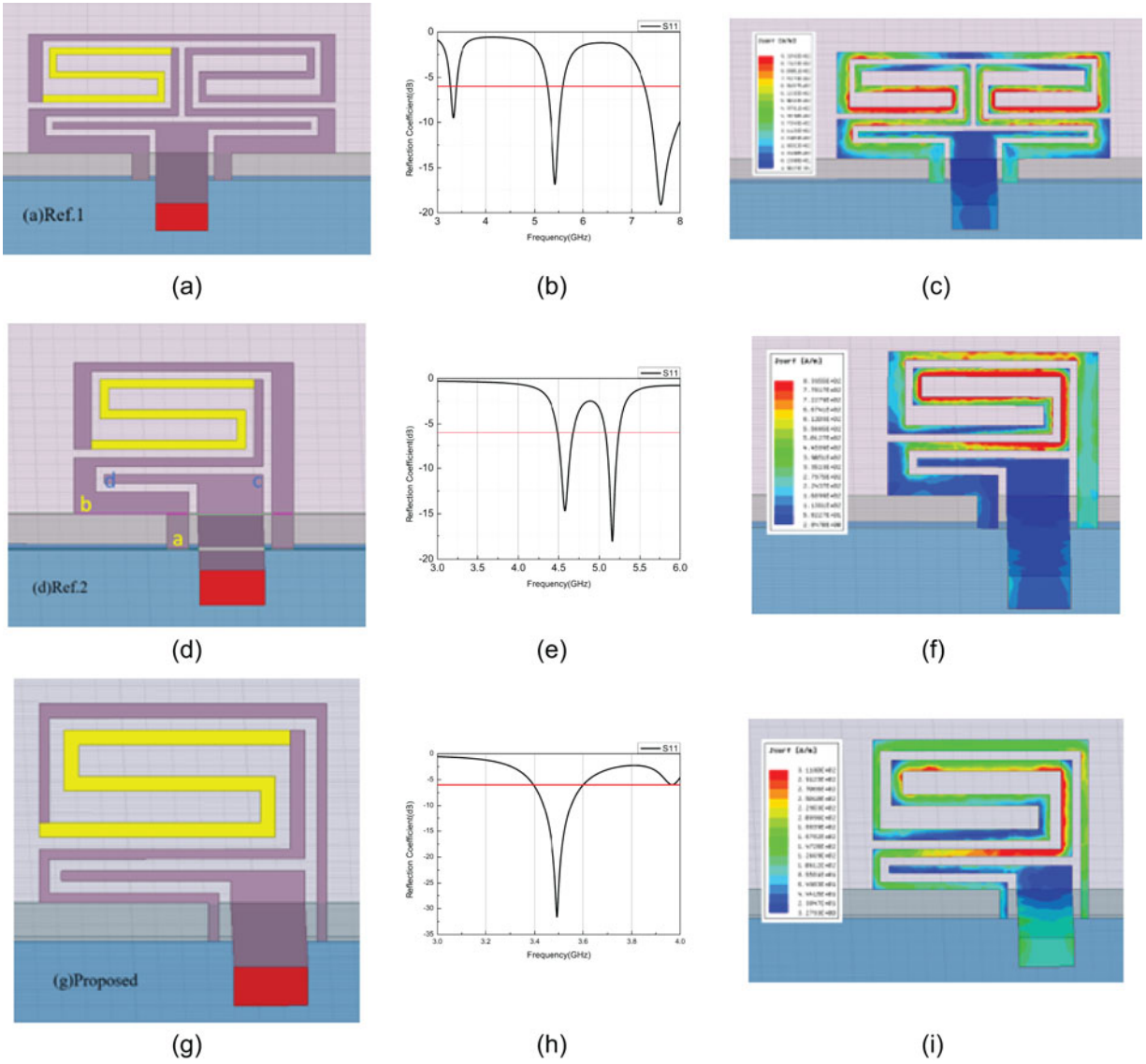


Figure 3. The antenna design process shows (a) Ref. 1, (d) Ref. 2, and (g) the proposed Ant. The reflection coefficients are for (b) Ref. 1, (e) Ref. 2, and (h) the proposed Ant. The current distributions are for (c) Ref. 1, (f) Ref. 2, and (i) the proposed Ant.

https://doi.org/10.1017/S1759078723000673 Published online by Cambridge University Press

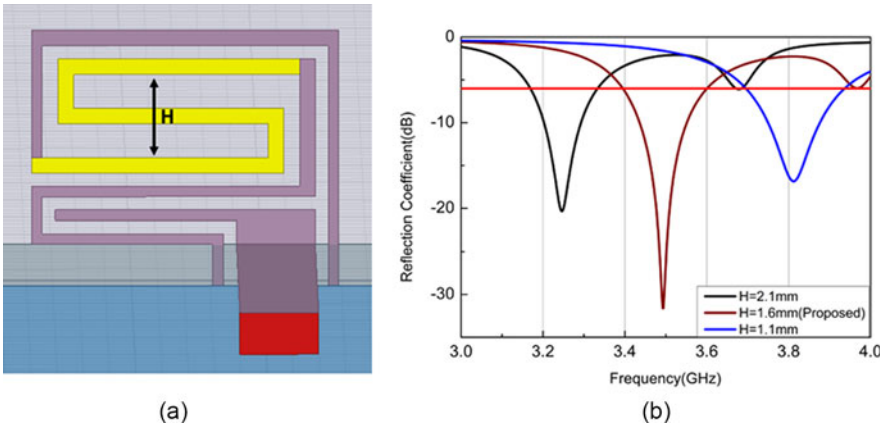


Figure 4. (a) The parameter *H* for the proposed antenna and (b) the variation in the reflection coefficient as *H* varies.

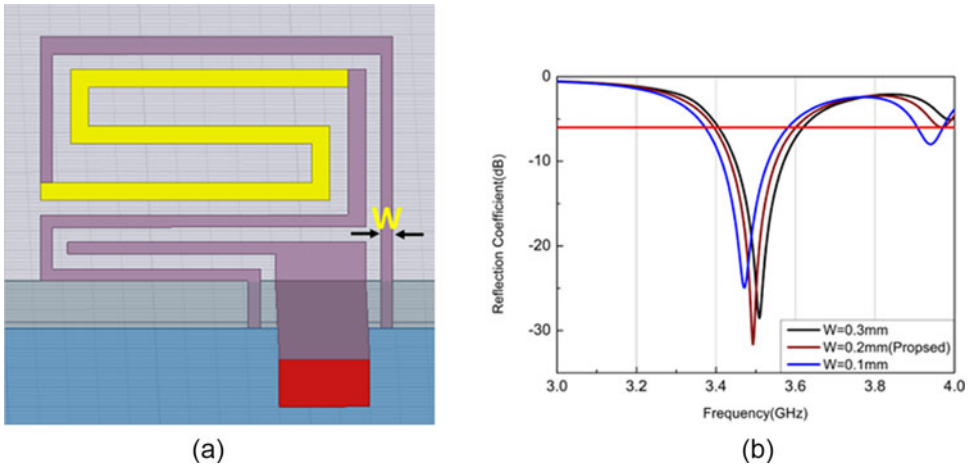


Figure 5. (a) The parameter *W* for the proposed antenna and (b) variation in the reflection coefficient as *W* varies.

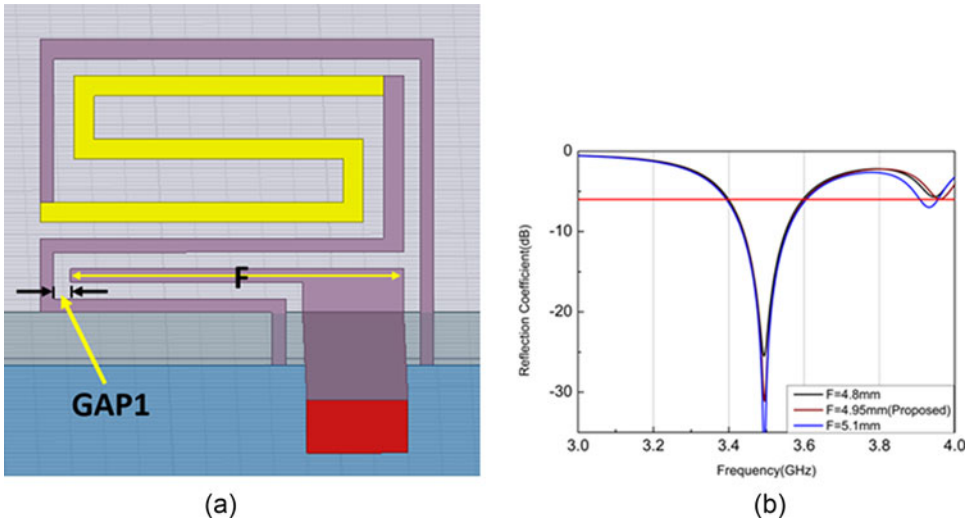


Figure 6. (a) The parameter *F* for the proposed antenna and (b) variation in the reflection coefficient as *F* varies.

https://doi.org/10.1017/S1759078723000673 Published online by Cambridge University Press

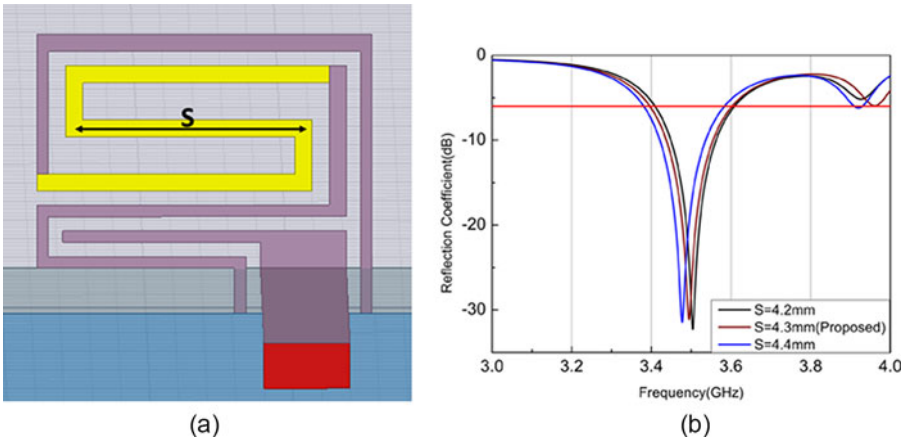


Figure 7. (a) The parameter *S* for the proposed antenna and (b) variation in the reflection coefficient as *S* varies.

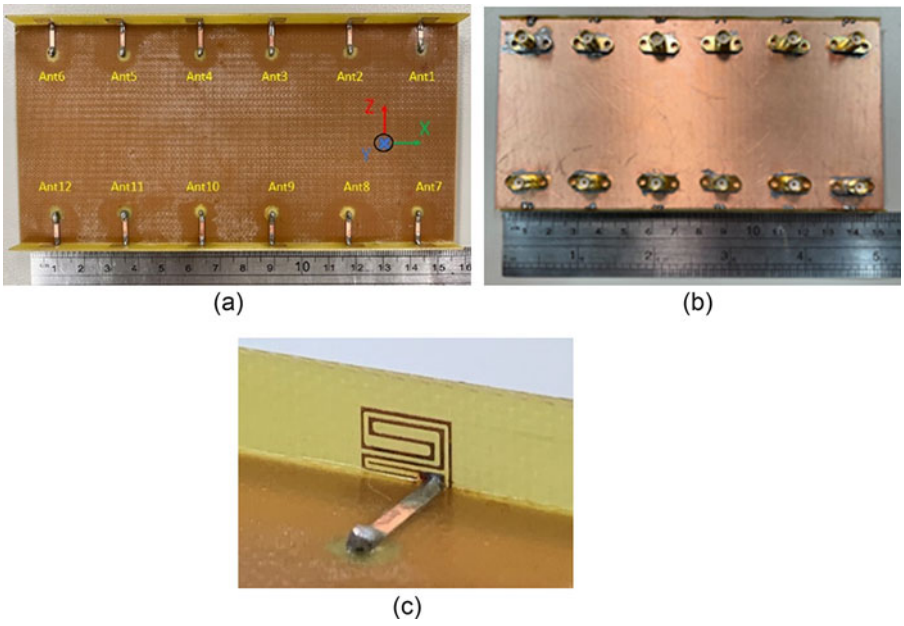


Figure 8. Photographs of the fabricated 12-element MIMO antenna: (a) front, (b) back, and (c) lateral view of the single antenna element.

adjacent antennas. The measured 6-dB impedance bandwidth is from 3.4 to 3.73 GHz and covers the long-term evolution 42 (LTE42) (3.4–3.6 GHz) band.

Design for the proposed antenna

Antenna structure and principle

Figure 1(a) shows the positions of antennas for a MIMO antenna array in a mobile phone. The size of the mobile phone is 150 mm (length) × 75 mm (width) × 7 mm (height). The blue part on the back of the FR4 substrate that is 0.8 mm thick is the system ground plane ($\varepsilon_r = 4.4, \tan\delta = 0.02$). The antennas for the proposed 12 × 12 MIMO antenna array are placed on two side edges of the mobile phone. Figure 1(b) and (c) shows the geometric and the detail parameters for the proposed single antenna element. Figure 1(b) and (c), respectively, shows the front view and the lateral view of the proposed single antenna element. The single antenna

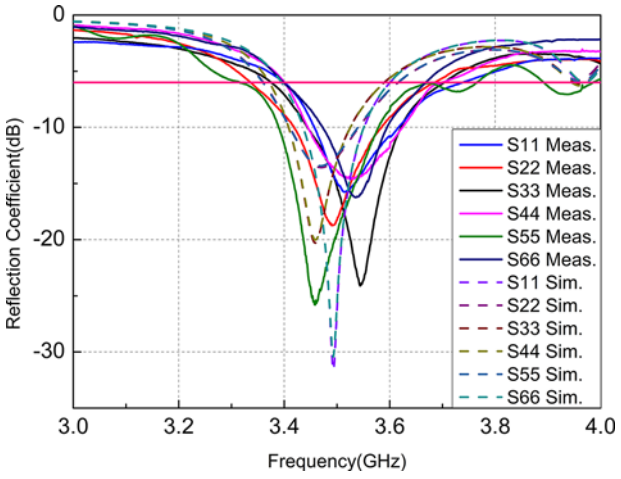


Figure 9. Reflection coefficients for simulation and measurement.

https://doi.org/10.1017/S1759078723000673 Published online by Cambridge University Press

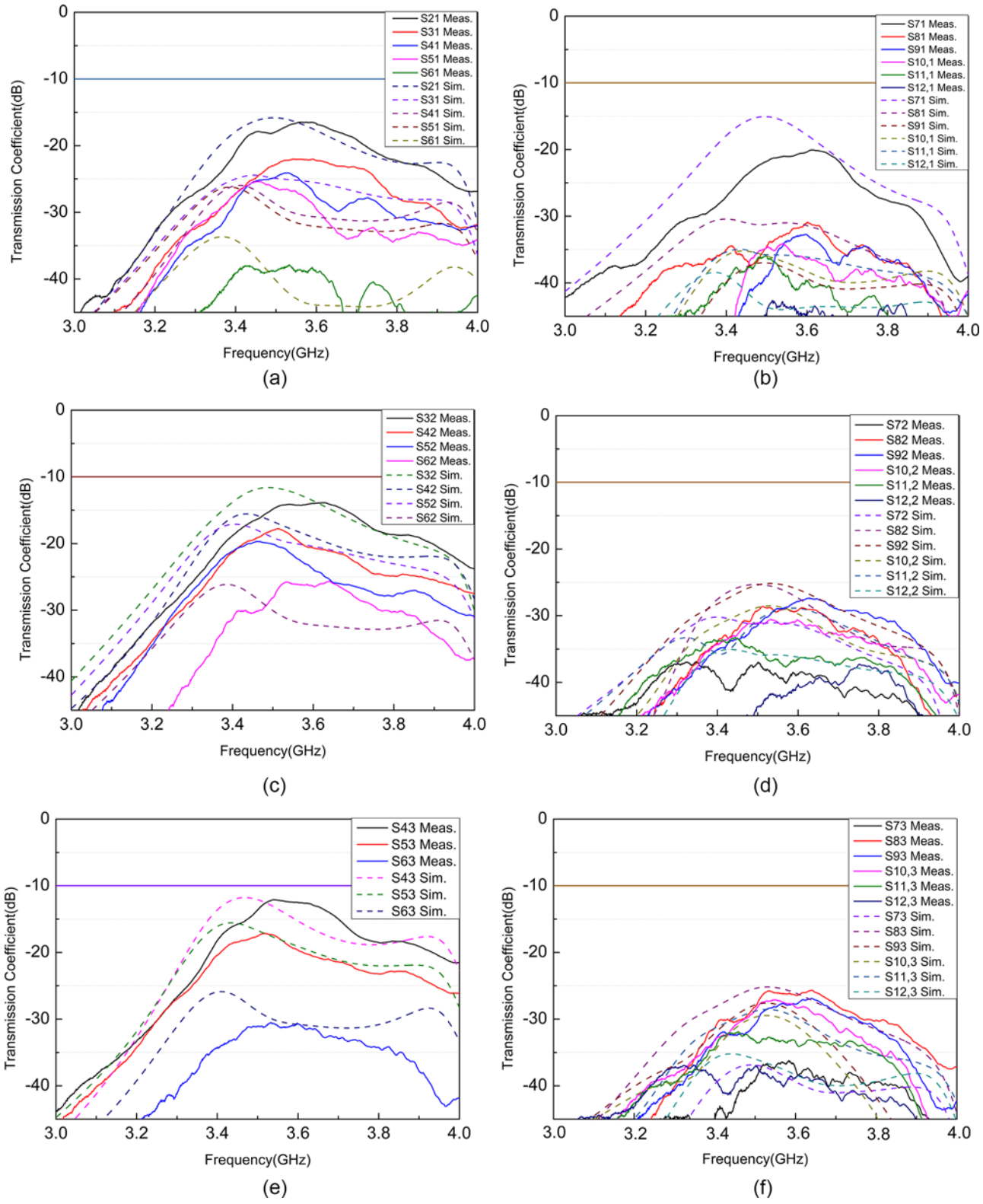


Figure 10. Transmission coefficients for simulation and measurement (a) between Ant1 and Ant2 to 6, (b) between Ant1 and Ant7 to 12, (c) between Ant2 and Ant3 to 6, (d) between Ant2 and Ant7 to 12, (e) between Ant3 and Ant4 to 6, and (f) between Ant3 and Ant7 to 12.

element is composed of a serpentine-structure loop antenna and an inverted-L feeding structure. The serpentine-structure loop antenna has a resonance frequency of 3.5 GHz. The length of the loop antenna is 43.8 mm, which is around half the wavelength of 3.5 GHz.

The inverted-L feeding structure, which is a capacitive coupling structure, is connected to a 50 Ω transmission line. In Fig. 1(b) and (c), the red rectangle is the feeding point for the proposed antenna and the blue area is the ground plane in the mobile phone. The size of a single antenna element is 5.85×4.9 mm^2 ($0.068\lambda_0 \times 0.057\lambda_0$).

https://doi.org/10.1017/S1759078723000673 Published online by Cambridge University Press

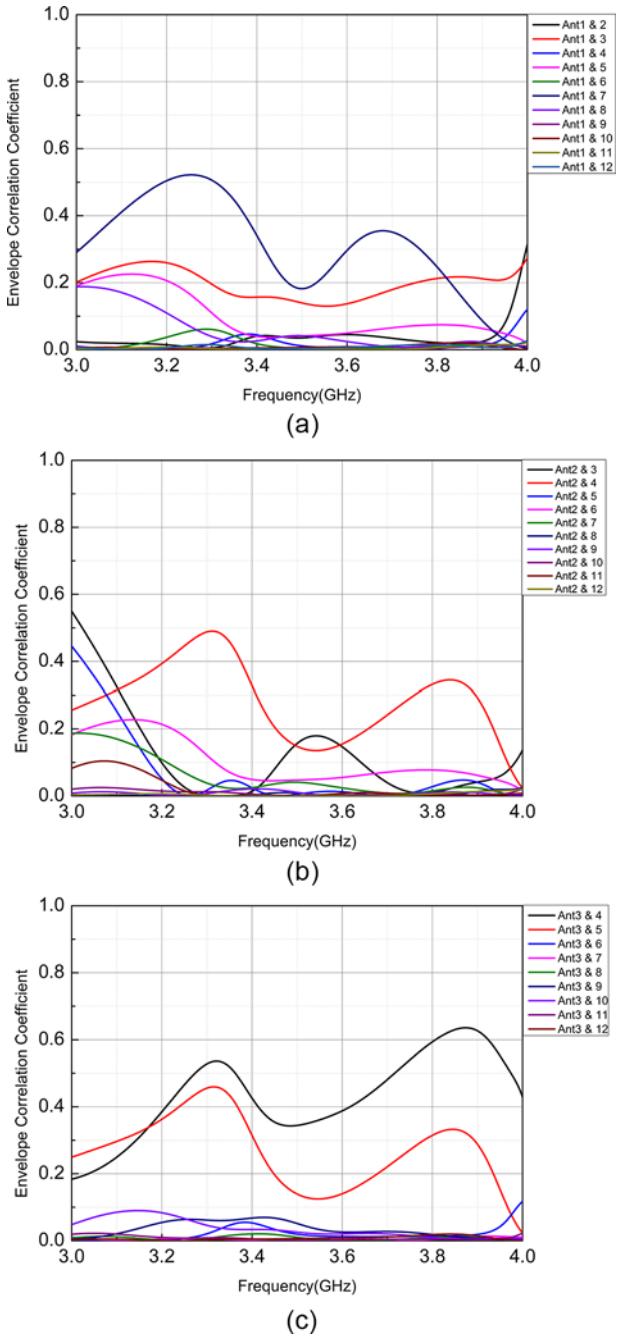


Figure 11. Calculated ECC values for (a) Ant1, (b) An2, and (c) Ant3 to other antennae.

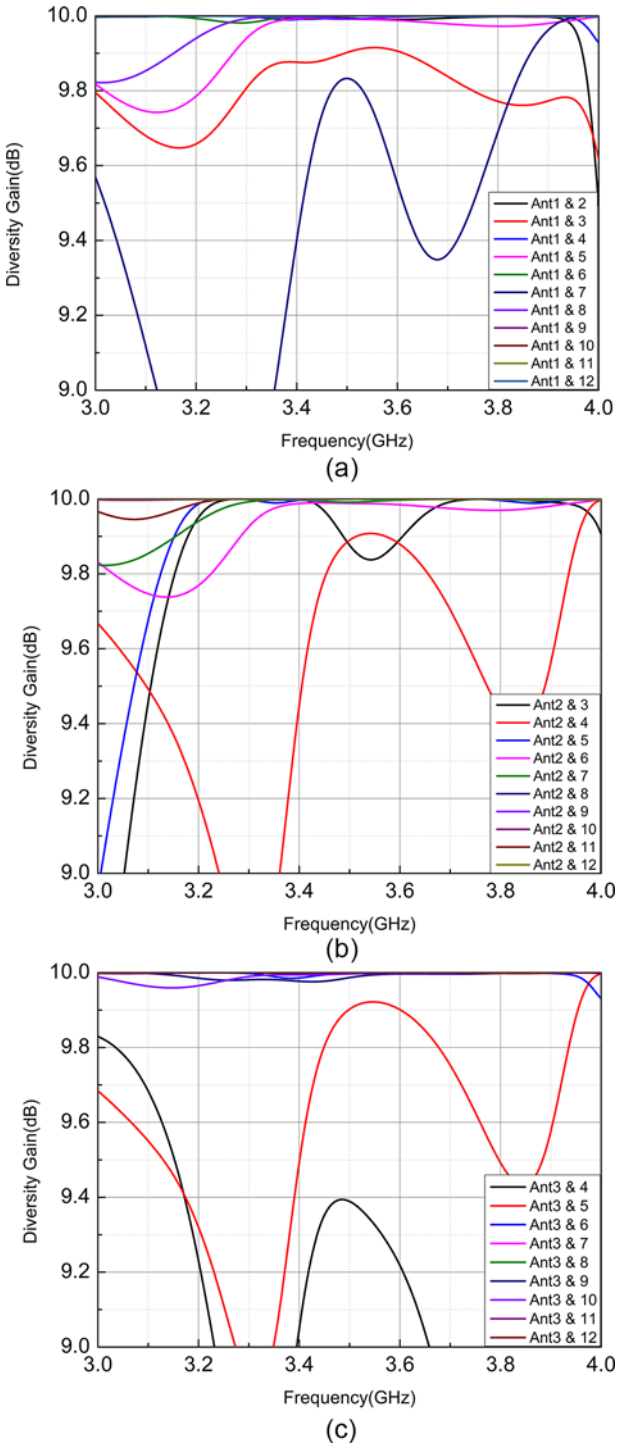


Figure 12. Calculated DG values for (a) Ant1, (b) Ant2, and (c) Ant3 to other antennae.

The width of all lines for the proposed antenna is 0.2 mm, except lines that are marked with a yellow T, which are 0.3 mm, and all gaps between line and line of the antenna are 0.25 mm except for gaps that are marked with a red G, which are 0.3 mm, as shown in Fig. 1(c). The simulated reflection coefficients for the proposed MIMO antenna array are shown in Fig. 2, and the 6-dB impedance bandwidth covers 3.4–3.6 GHz.

Antenna design process and current distribution

In Fig. 3(a), the bilateral-symmetry serpentine loop antenna, which is called Ref.1, initially had a T-shape feeding structure. Ref.1 excites three resonating modes at around 3.3, 5.4, and 7.5 GHz and the reflection coefficient is shown in Fig. 3(b). Ref.1 is a bilateral-symmetry structure, so the current distribution is 5.4 GHz on the right-hand side and the left-hand side of Ref.1, as shown in Fig. 3(c). Therefore, Ref.1 can be divided into two identical half-antennas. The half-antenna that is fed by an L-shape feeding structure and is connected by a straight strip to the ground is called Ref.2, as shown in Fig. 3(d). The L-shape feeding structure in Ref.2

https://doi.org/10.1017/S1759078723000673 Published online by Cambridge University Press

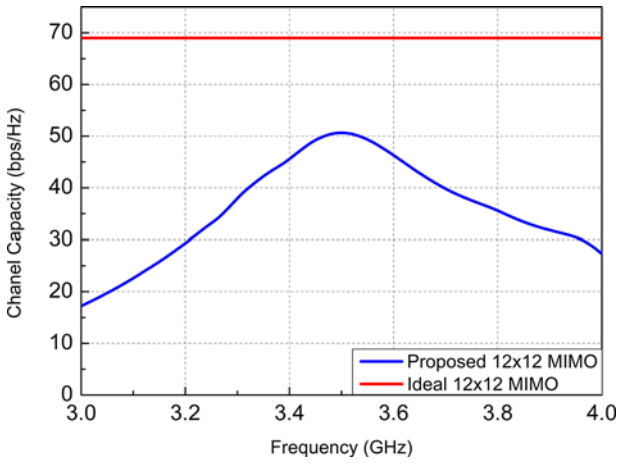


Figure 13. Calculated channel capacity for the proposed MIMO antenna array.

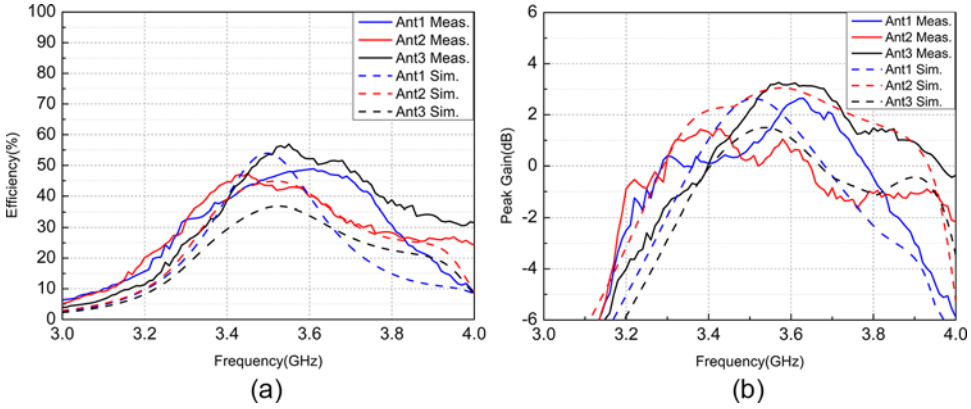


Figure 14. Simulated and measured (a) total efficiency and (b) peak gain.

is split from the T-shape feeding structure in Ref.1. The L-shape feeding structure is compressed, so line ab and line cd are shorter, as shown in Fig. 3(d).

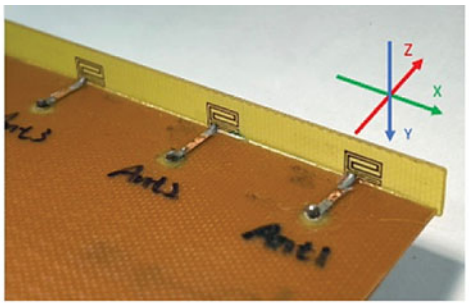
Ref.2 uses a straight strip that is connected to the ground, so Ref.2 is longer than half of the length of Ref.1. Therefore, the first resonant frequency of Ref.2 is lower than the second resonant frequency of Ref.1. The first resonant frequency for Ref.2 is 4.6 GHz and the length of the current path, which is about $0.5\lambda_0$ at 4.6 GHz, is 32 mm, as shown in Fig. 3(e). However, the operating band is still not close to the desired band of 3.4–3.6 GHz. Extending the length of the current path for Ref.2 forms the proposed antenna, as shown in Fig. 3(g). The size of the proposed antenna is also increased to 5.85×4.9 mm^2. The reflection coefficient for the proposed antenna is shown in Fig. 3(h). The resonant frequency is around 3.5 GHz, and the operating bandwidth covers the required band of 3.4–3.6 GHz. The current distribution for the proposed antenna at 3.5 GHz is shown in Fig. 3(i). The length of the proposed antenna is 43.8 mm, which is half of the wavelength for the resonant frequency of 3.5 GHz.

Parametric analysis

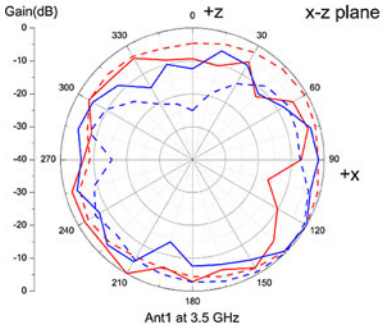
The parameter H, which is the distance between the upper and lower arms of the S-shaped strip line for the proposed antenna, is shown in Fig. 4(a). The reflection coefficients are specified relative to the variations in the parameter H, as shown in Fig. 4(b). As the value for the parameter H increases, the current path becomes longer and the resonant frequency decreases. As the value of the parameter H decreases, the resonance frequency shifts increase. Therefore, a value for H of 2.1 mm equates to the lowest resonance frequency of 3.25 GHz and a value for H of 1.1 mm equates to a resonating frequency of 3.8 GHz. The optimal value for H is 1.6 mm because the 6-dB impedance frequency covers the desired band.

The width (parameter W) of the straight shorting line that is connected to the ground is also studied, as shown in Fig. 5(a). The value of the parameter W is used to fine-tune the resonance frequency. As W becomes wider, the resonance frequency increases slightly. The optimal value for parameter W is 0.2 mm because the 6-dB impedance bandwidth is from 3400 to 3730 MHz and covers 3400–3600 MHz, as shown in Fig. 5(b). Adjusting the length (parameter F) of the L-shaped feeding structure in Fig. 6(a) affects the impedance matching. From Fig. 6(b), it can be observed that the longer parameter F has better impedance matching. However, a greater value for parameter F creates a small value for gap1, which is the gap between the feeding structure and the serpentine antenna, as shown in Fig. 6(a). gap1 is too small to be fabricated so the optimal value for the parameter F is 4.95 mm and impedance matching is sufficient (reflection coefficient is around −30 dB). The value for the parameter S (Fig. 7(a)) is used to fine-tune the operating frequency such as the parameter W, as shown in Fig. 7(b). As the value for the parameter S is increased, the resonance frequency

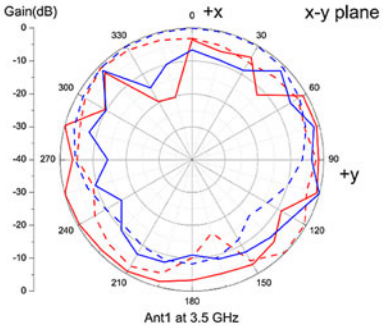
https://doi.org/10.1017/S1759078723000673 Published online by Cambridge University Press



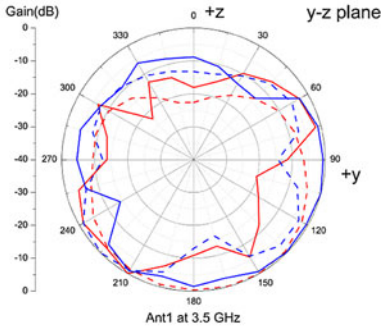




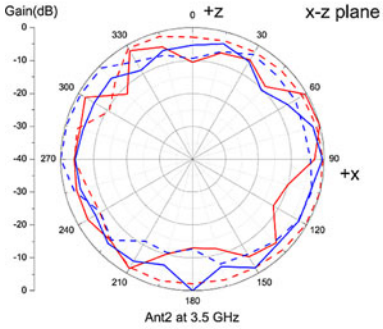
(a)



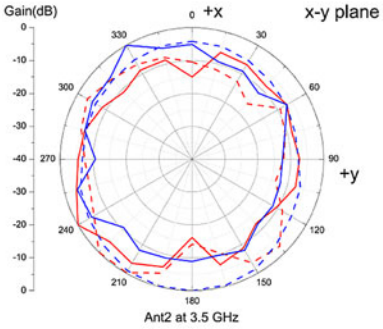
(b)



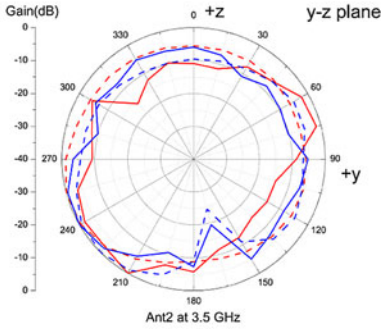
(c)



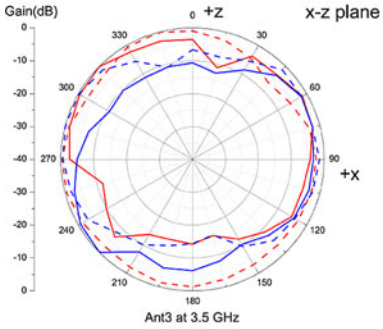
(d)



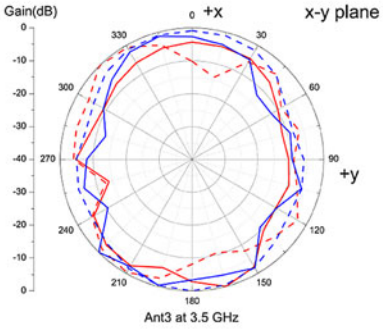
(e)



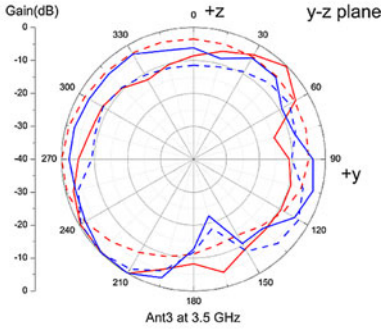
(f)



(g)



(h)



(i)

Figure 15. Simulated and measured radiation patterns for the proposed MIMO antenna at 3.5 GHz: (a) *xz*-plane, (b) *xy*-plane, and (c) *yz*-plane for Ant1, (d) *xz*-plane, (e) *xy*-plane, and (f) *yz*-plane for Ant2, and (g) *xz*-plane, (h) *xy*-plane, and (i) *yz*-plane for Ant3.

https://doi.org/10.1017/S1759078723000673 Published online by Cambridge University Press

decreases slightly. The optimal value for the parameter S is 4.3 mm, and the 6-dB impedance bandwidth covers the LTE42 band.

Measurements and discussion

Figure 8(a–c) shows front, rear, and lateral views of the proposed MIMO antenna. The simulated and measured reflection coefficients for Ant1 to Ant6 are shown in Fig. 9. The solid lines in Fig. 9 are measurements and the dotted lines are simulations. The MIMO antenna is symmetrical, so only Ant1 to Ant6 are measured. All of the measured reflection coefficients are similar to the simulated results, but the frequency shifts slightly. The 6-dB impedance bandwidth for the entire antenna covers the LTE42 band.

Figure 10 shows simulated and measured transmission coefficients for Ant1, Ant2, and Ant3 to other antennae. Only the transmission coefficients between Ant1 to Ant3 and other antennae are shown because the arrangement of those antennas is symmetrical in the mobile phone. Figure 10(a) and (b) shows the simulated and measured transmission coefficients between Ant1 and other antennae. Figure 10(c) and (d) shows the simulated and measured transmission coefficients between Ant2 and other antennae. Figure 10(e) and (f) shows the simulated and measured transmission coefficients between Ant3 and other antennae. All of the measured transmission coefficients are less than −12 dB. Figure 10 shows that there is good agreement between the measured and simulated results.

The performance of the proposed MIMO antenna is determined using the envelope correlation coefficient (ECC) and the diversity gain (DG). The ECC represents the degree of correlation between the signal that is received by different antenna elements and DG measures the benefits of having multiple uncorrelated signals in the system [26]. ECC and DG are, respectively, defined as (1) and (2):

$$\rho_e = \frac{\left| \int\int \vec{E}_i(\theta,\phi)\vec{E}_j(\theta,\phi)\mathrm{d}\Omega \right|^2}{\left|\vec{E}_i(\theta,\phi)\right|^2 \left|\vec{E}_j(\theta,\phi)\right|^2 \mathrm{d}\Omega}, \quad (1)$$

$$\mathrm{DG} = 10\sqrt{1-\rho_e^2} \quad (2)$$

[27]. Figure 11(a–c), respectively, shows the calculated values for ECC for Ant1, Ant2, and Ant3 to other antennae. These ECC values are less than 0.42 at 3.4–3.6 GHz. Figure 12(a–c), respectively, show the calculated DG values for Ant1, Ant2, and Ant3 to other antennas. The DG values are more than 9 dB at 3.4–3.6 GHz. The ergodic CC for the proposed MIMO antenna is determined using Equation (3) as [12, 28]:

$$\mathrm{CC} = E\left\{\log_2\left[\det\left(I + \frac{\mathrm{SNR}}{m_{\mathrm{tr}}}\right)\mathrm{HH}^{\mathrm{T}}\right]\right\}. \quad (3)$$

In Equation (3), an equal amount of power is allocated to each transmit antenna, but there is no prior knowledge of the channel state information included. The calculated CC value for the proposed MIMO antenna is between 45 and 50 bps/Hz at 3.4–3.6 GHz, as shown in Fig. 13. Figure 14 shows the simulated and measured total efficiency and peak gain for Ant1 to Ant3. The MIMO antenna is symmetrical so only Ant1 to Ant3 are shown. The simulated total efficiency for the proposed MIMO antenna is between 40% and 57%, and the measured total efficiency for the proposed MIMO antenna is between 39% and 56%, as shown in Fig. 14(a). Figure 14(b) shows that the simulated and measured peak gain for the proposed MIMO antenna is between 1 and 2.6 dBi and between 0 and 3.2 dBi, respectively.

The 2D normalized radiation pattern for Ant1 to Ant3 in the *xz*-, *yz*-, and *xy*-planes at 3.5 GHz is shown in Fig. 15. Figure 15(a–c) shows the radiation patterns for Ant1 in the *xz*-, *yz*-, and *xy*-planes at 3.5 GHz. Figure 15(d–f) shows the radiation patterns for Ant2, and Fig. 15(g–i) shows the radiation patterns for Ant3. The loop antenna is a magnetic dipole so the $E\phi$ value for Ant1 to Ant3 in the *xz*-plane features an omnidirectional radiation pattern, as shown in Fig. 15(a), (d), and (g).

Conclusion

A compact 12 × 12 MIMO loop antenna array is proposed for 5 G mobile phone applications. The single antenna element uses a fold and serpentine design to reduce the size, which is 5.85 × 4.9 mm^2 ($0.068\lambda_0 \times 0.057\lambda_0$). The MIMO antenna has a small transmission coefficient of less than −12 dB, and no decoupling element is used. The measured 6-dB impedance bandwidth for the antenna is 3.4–3.73 GHz and covers the LTE 42 (3.4–3.6 GHz) band. The measured total efficiency for the proposed antenna is 39–56%. The ECC value is less than 0.42, the CC is 45–50 bps/Hz, and the peak gain is 0–3.2 dBi.

Funding Statement. The authors would like to thank the Ministry of Science and Technology (Taiwan) and National Pingtung University for partially sponsoring this study. The project number for the MOST is MOST 106-2633-E-153-001.

Competing interests. The authors report no conflict of interest.

References

1. **Dubazane SP, Kumar P and Afullo TJO** (2022) Metasurface superstrate-based MIMO patch antennas with reduced mutual coupling for 5G communications. *The Applied Computational Electromagnetics Society Journal (ACES)* **37**, 408–419.
2. **Dubazane S, Kumar P and Afullo TJO** (2021) Metasurface based MIMO microstrip antenna with reduced mutual coupling. In 2021 IEEE AFRICON, Arusha, United Republic of Tanzania, 1–7.
3. **Parchin NO, Al-Yasir YIA, Abdulkhaleq AM, Basherlou HJ, Ullah A and Abd-Alhameed RA** (2020) A new broadband MIMO antenna system for Sub 6 GHz 5G cellular communications. In 2020 14th European Conference on Antennas and Propagation (EuCAP), Copenhagen, Denmark, 1–4.
4. **Al-Bawri S, Islam M, Singh M, Alyan E, Jusoh M, Sabapathy T, Padmanathan S and Hossain K** (2021) Broadband Sub-6GHz Slot-based MIMO antenna for 5G NR bands mobile applications. *Journal of Physics: Conference Series* **1962**, 012038.
5. **Sheriff N, Kamal S, Tariq Chattha H, Kim Geok T and Khawaja BA** (2022) Compact wideband four-port MIMO Antenna for Sub-6 GHz and internet of things applications. *Micromachines* **13**, 2202.
6. **Liao SM** (2021) MIMO antenna with decoupled antenna Pairs for 5G mobile terminals. In 2021 Cross Strait Radio Science and Wireless Technology Conference (CSRSWTC), Shenzhen, China, 120–122.
7. **Serghiou D, Khalily M, Singh V, Araghi A and Tafazolli R** (2020) Sub-6 GHz dual-band 8 × 8 MIMO antenna for 5G smartphones. *IEEE Antennas and Wireless Propagation Letters* **19**, 1546–1550.
8. **Wong K, Tsai C and Lu J** (2017) Two asymmetrically mirrored gap-coupled loop antennas as a compact building block for eight-antenna MIMO array in the future smartphone. *IEEE Transactions on Antennas and Propagation* **65**, 1765–1778.

https://doi.org/10.1017/S1759078723000673 Published online by Cambridge University Press

9. **Alja'afreh SS** (2021) Ten antenna array using a small footprint capacitive-coupled-shorted loop antenna for 3.5 GHz 5G smartphone applications. *IEEE Access* **9**, 33796–33810.
10. **Piao H, Jin Y and Qu L** (2020) A compact and straightforward self-decoupled MIMO antenna system for 5G Applications. *IEEE Access* **8**, 129236–129245.
11. **Zhao A and Ren Z** (2019) Wideband MIMO antenna systems based on coupled-loop antenna for 5G N77/N78/N79 applications in mobile terminals. *IEEE Access* **7**, 93761–93771.
12. **Ahmad U** (2021) MIMO antenna system with pattern diversity for Sub-6 GHz mobile phone applications. *IEEE Access* **9**, 149240–149249.
13. **Guo J, Cui L, Li C and Sun B** (2018) Side-edge frame printed eight-port dual-band antenna array for 5G smartphone applications. *IEEE Transactions on Antennas and Propagation* **66**, 7412–7417.
14. **Wang S** (2019) Design of a twelve-port MIMO Antenna for 5G/4G Smartphone Application. In 2019 International Symposium on Antennas and Propagation (ISAP).
15. **Ren Z, Zhao A and Wu S** (2019) MIMO antenna with compact decoupled Antenna Pairs for 5G mobile terminals. *IEEE Antennas and Wireless Propagation Letters* **18**, 1367–1371.
16. **Xu Z and Deng C** (2020) High-Isolated MIMO antenna design based on pattern diversity for 5G Mobile Terminals. *IEEE Antennas and Wireless Propagation Letters* **19**, 467–471.
17. **Liu Y, Zhao X, Jing G, He Y, Xi M and Zhao L** (2019) Three ways to decouple multiple antennas in a Mobile Terminal. In 2019 International Symposium on Antennas and Propagation (ISAP).
18. **Muhsin MY, Salim AJ and Ali JK** (2021) An Eight-Element MIMO Antenna system for 5G Mobile Handsets. In 2021 International Symposium on Networks, Computers and Communications (ISNCC), Dubai, United Arab Emirates.
19. **Alwarafy A, Sulyman AI, Alsanie A, Alshebeili S and Behairy H** (2015) Receiver spatial diversity propagation path-loss model for an indoor environment at 2.4 GHz. In 2015 6th International Conference on the Network of the Future (NOF).
20. **İncesulu H, Ulutaş G, Bilge H, İmeci ŞT and Durak T** (2017) F-shaped monopole antenna. In 2017 International Applied Computational Electromagnetics Society Symposium—Italy (ACES).
21. **Park E, Yoon YJ and Kim H** (2018) Dual polarization L-Shaped slot array antenna for 5G Metal-Rimmed Mobile Phone, 2018. In International Symposium on Antennas and Propagation (ISAP).
22. **Mok WC, Wong SH, Luk KM and Lee KF** (2013) Single-layer single-patch dual-band and triple-band patch antennas. *IEEE Transactions on Antennas and Propagation* **61**, 4341–4344.
23. **Wang Y and Du Z** (2013) A wideband printed dual-antenna system with a novel neutralization line for mobile terminals. *IEEE Antennas and Wireless Propagation Letters* **12**, 1428–1431.
24. **Vaughan RG** (1990) Polarization diversity in mobile communications. *IEEE Transactions on Vehicular Technology* **39**, 177–186.
25. **Zhuang X, Feng Z and Wu D** (2015) Strongly coupled array elements decoupled by Eigen-mode analysis and its affection on radiate property. In 2015 IEEE International Wireless Symposium (IWS 2015).
26. **Malviya L, Panigrahi RK and Kartikeyan M** (2017) MIMO antennas with diversity and mutual coupling reduction techniques: A review. *International Journal of Microwave and Wireless Technologies* **9**, 1763–1780.
27. **Mashagba HA** (2021) A hybrid mutual coupling reduction technique in a Dual-Band MIMO textile antenna for WBAN and 5G Applications. *IEEE Access* **9**, 150768–150780.
28. **Ullah R, Ullah S, Faisal F, Ullah R, Mabrouk IB, Hasan MJA and Kamal B** (2021) A novel multi-band and multi-generation (2G, 3G, 4G, and 5G) 9-elements MIMO antenna system for 5G smartphone applications. *Wireless Networks* **27**, 4825–4837.



Ji-Peng Jhuang received his B.S. degree in the Department of Computer and Communication from National Pingtung University, Taiwan, in 2021. In 2022, he joined the Department of Computer Science and Information Engineering, Taiwan. His research interests include MIMO antenna design, fabrication, and measurements, as well as Sub-6-GHz band and mobile phone antennas. His current research interests involve the design of access point antennas, dual-polarization antennas, and MIMO loop slot antennas for Sub-6-GHz applications.



Hsin-Lung Su was born in Kaohsiung, Taiwan. He received the B.S. degree in electronic engineering from National Taiwan Institute of Technology, Taipei, and the M.S. and Ph.D. degrees in electrical engineering from National Sun Yat-Sen University (NSYSU), Kaohsiung, Taiwan. From 2007 to 2013, he was with the Department of Computer and Communications, National Pingtung Institute of Commerce, Pingtung, Taiwan. He has been serving in the Department of Computer and Communications, National Pingtung University (NPTU) since 2013. He is currently an Associate Professor with NPTU. His current research interests include antennas, metamaterials, metamaterial-inspired structures, EBG structures, conducted emission of electromagnetic compatibility, and the application of EM waves of the anisotropic media. Dr. Su serves as the Vice Chair in APSTNC (IEEE Antennas and Propagation Society Tainan Chapter) from 2016 to 2022. Now, he serves as the Chair in APSTNC.

https://doi.org/10.1017/S1759078723000673 Published online by Cambridge University Press